

# Combining directional light output and ultralow loss in deformed microdisks

Jan Wiersig

*Institut für Theoretische Physik, Universität Bremen, Postfach 330 440, D-28334 Bremen, Germany*

Martina Hentschel

*Max-Planck-Institut für Physik komplexer Systeme, Nöthnitzer Str. 38, D-01187 Dresden, Germany*

(Dated: October 24, 2018)

A drawback of high-quality modes in optical microdisks is their isotropic light emission characteristics. Here we report a novel, robust, and general mechanism that results in highly directional light emission from those modes. This surprising finding is explained by a combination of wave phenomena (wave localization along unstable periodic ray trajectories) and chaotic ray dynamics in open systems (escape along unstable manifolds). The emission properties originating in the chaotic ray dynamics permit directional light output even from microlasers operating in the common multi-mode regime. We demonstrate our novel mechanism for the limaçon billiard family and find directional emission with narrow angular divergence for a significant range of geometries and material parameters.

PACS numbers: 42.55.Sa, 42.25.-p, 42.60.Da, 05.45.Mt

The possibility to confine photons in all three spatial dimensions using microcavities has triggered intense basic and applied research in physics over the past decade [1], e.g., research on ultralow threshold lasing [2, 3], single-photon emitters [4], solid-state cavity quantum electrodynamics [5, 6, 7]. Prominent examples of optical microcavities are whispering-gallery cavities such as microdisks [8, 9], microspheres [10, 11, 12], and microtori [13, 14] which trap photons for a long time  $\tau$  near the boundary by total internal reflection. The corresponding whispering-gallery modes have very high quality factors  $Q = \omega\tau$ , where  $\omega$  is the resonance frequency. For microdisks, the record  $Q$ -factor is around  $6.6 \times 10^5$  [9]. The high  $Q$ -factors and the in-plane light emission make microdisks attractive candidates for several optoelectronic devices, especially for the nitride material system [15] where other cavity designs such as vertical-cavity surface-emitting laser (VCSEL) micropillars faces severe challenges in mirror fabrications [16]. Unfortunately, the possible use of microdisks is limited by the fact that the in-plane light emission is isotropic.

Shortly after the first fabrication of semiconductor microdisk resonators it has been demonstrated that deforming the boundary of a disk allows for improved directionality of emission and therefore for more efficient extraction and collection of light [17, 18, 19, 20]. Several shapes have been proposed and realized since then, but only few lead to light emission into a single direction with reasonable angular divergence [21, 22] that is essential for applications like single-photon sources. Moreover, all deformed microdisks discussed in the literature have a serious problem,  $Q$  spoiling [23]: The  $Q$ -factor degrades dramatically upon deformation; in the worst case ruling out any application. The trade-off between  $Q$ -factor and directionality is not only a problem of microdisks but also of microspheres, microtori, and even of VCSEL-micropillars: for given total number of Bragg mirror pairs such a cavity can be optimized either w.r.t. directionality (significantly more mirror pairs at the bottom than at the top) or  $Q$ -factor (roughly equal number of mirror pairs at the bottom and top).

Recently, a scheme to achieve highly directional emission

without  $Q$ -spoiling has been suggested [24]. It employs the characteristic modifications of spatial mode structures near avoided resonance crossings. The drawback of this approach is the existence of nearly degenerate modes which can have different far-field patterns (FFPs). If two such modes are excited simultaneously (typical for present-day devices), the directionality might be lost. Nearly degenerate modes with similar FFP do occur but to find them requires laborious numerical calculations and a sophisticated adjustment of geometry parameters depending on refractive index, wavelength and cavity size.

In this Letter we introduce a novel, robust, and generally applicable mechanism to achieve highly directional light emission from high- $Q$  modes in microdisks which does not suffer from the above-mentioned drawback. The key to our finding is to apply what is at the heart of quantum chaos [25] and nonlinear dynamics [26] of open systems, respectively: wave localization along unstable periodic ray trajectories in systems with chaotic ray dynamics [27] and the only recently acknowledged importance of the so-called unstable manifold for the FFPs of microcavities [28, 29, 30, 31]. The wave localization ensures the desired high  $Q$ -factors, whereas the unstable manifold provides the directional emission. Concerning the realisation of this scheme in practise, adequate microcavity devices can be expected to be easy to fabricate as no sophisticated adjustment of parameters is required. They are, moreover, well suited for multi-mode laser operation as all high- $Q$  modes of given polarization possess similar FFPs.

A microdisk is a quasi-two-dimensional geometry described by an effective index of refraction  $n$ . We assume  $n = 3.3$  (GaAs) both for transverse magnetic (TM) and transverse electric (TE) polarization. A slight polarization dependence of  $n$  is neglected; it could be adjusted in the fabrication process, e.g., by changing the slab thickness. For the boundary curve of the deformed microdisk we choose the limaçon of Pascal which reads in polar coordinates  $(\rho, \phi)$

$$\rho(\phi) = R(1 + \varepsilon \cos \phi). \quad (1)$$

The corresponding family of closed cavities is known as

“limaçon billiards” [32]. Ray and wave dynamics in billiards has been extensively discussed in the fields of nonlinear dynamics [26] and quantum chaos [25]. The limiting case of vanishing deformation parameter  $\varepsilon$  is the circle with radius  $R$ . Figure 1(a) illustrates a whispering-gallery ray trajectory in a circular microdisk trapped by total internal reflection. A two-dimensional phase space representation, the so-called Poincaré surface of section (SOS), is shown in Fig. 1(b). Whenever the trajectory hits the cavity’s boundary, its position  $s$  (arclength coordinate along the circumference) and tangential momentum  $\sin \chi$  (the angle of incidence  $\chi$  is measured from the surface normal) is recorded. For  $\varepsilon = 0$ , rotational invariance of the system implies conservation of the angular momentum  $\propto \sin \chi$ . Ignoring wave effects, such a ray never leaves the cavity since it cannot enter the leaky region between the two critical lines for total internal reflection given by  $\sin \chi_c = \pm 1/n$ .

Figures 1(c) and (d) show a trajectory in the limaçon cavity for  $\varepsilon = 0.43$ . In contrast to the case of small deformation parameter  $\varepsilon$  [23] the dynamics is predominantly chaotic. Starting with an initial  $\chi$  well above the critical line, a test ray (square, thick dots, and triangle) rapidly approaches the leaky region ( $\sin \chi$  is not conserved) where it escapes according to Snell’s and Fresnel’s laws. Without refractive escape ( $n = \infty$ , hard wall or closed billiard limit), the trajectory would fill the phase space in a random fashion (small dots). Periodic ray trajectories do exist but are always unstable, except for the two islands in the leaky region. Whispering-gallery trajectories are confined to the tiny region  $|\sin \chi| \gtrsim 0.99$ .

While in the long-time limit the phase space of closed chaotic systems is essentially structureless, cf. Fig. 1(d), the phase space of an open chaotic system is structured by the so-called “chaotic repeller” [26]. It is the set of points in phase space that never visits the leaky region both in forward and backward time evolution. The stable (unstable) manifold of a chaotic repeller is the set of points that converges to the repeller in forward (backward) time evolution. The unstable manifold therefore describes the route of escape from the chaotic system. In the case of light, Fresnel’s laws impose an additional, polarization dependent weighting factor to the unstable manifold in the leaky region [31], since at each reflection the intensity inside is multiplied by the Fresnel reflection coefficient.

Following Refs. [29, 31] the unstable manifold can be uniquely computed as a survival probability distribution calculated from an ensemble of rays starting uniformly in phase space having identical intensity. Figure 2 depicts the resulting Fresnel weighted unstable manifolds for the limaçon cavity using 50 000 rays. Note that (i) in the leaky region, the manifold is concentrated on very few high-intensity spots. We therefore expect a highly directional FFP. (ii) While in the case of TE polarization one finds one spot with  $\chi > 0$  (and another symmetry-related one at  $s \rightarrow s_{\max} - s, \chi \rightarrow -\chi$ ), the TM polarization case possesses two of those.

The unstable manifold in the leaky region directly determines the FFP. Mapping the unstable manifold in Fig. 2 to the far field by using Snell’s and Fresnel’s laws (for generalization to curved interfaces, see [33]) we obtain Fig. 3. Note that

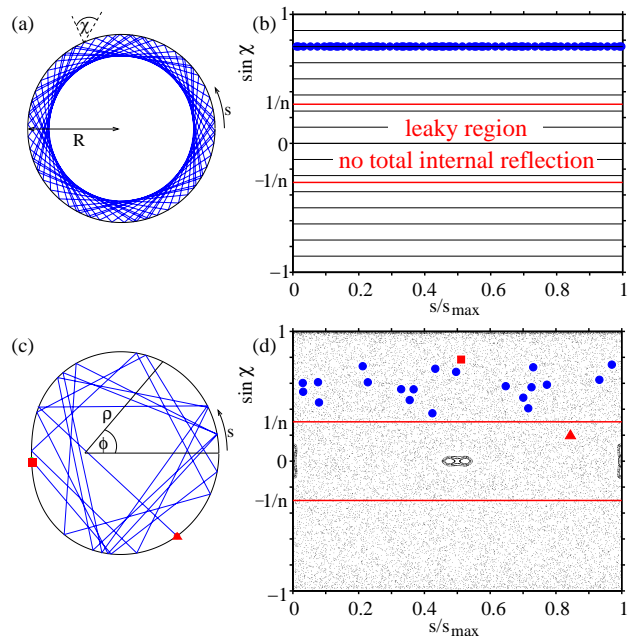


FIG. 1: (color online). (a) Whispering-gallery ray trajectory in the circular microdisk. (b) Poincaré SOS showing the trajectory (thick dots) in phase space;  $s$  is the arclength coordinate and  $\chi$  is the angle of incidence. Typical trajectories fill a line of constant  $\sin \chi$ . The critical lines  $\sin \chi_c = \pm 1/n$  enclose the leaky region. (c) Chaotic ray trajectory in the limaçon cavity (1) with  $\varepsilon = 0.43$ . (d) Poincaré SOS for the trajectory (thick dots) starting above the critical line (square) and refractively escaping after only 20 bounces (triangle). Small dots show a typical trajectory in the corresponding closed billiard system.

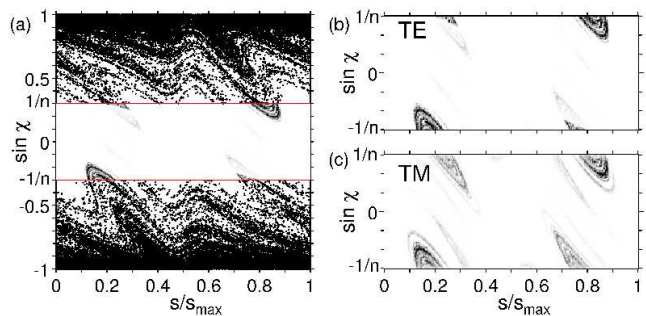


FIG. 2: (color online). (a) Fresnel weighted unstable manifold of the limaçon cavity for TE polarization. Magnification reveals the differences between TE (b) and TM (c) polarization in the leaky region, which originate from Fresnel’s law.

the FFP is shown only for the upper half space ( $0^\circ - 180^\circ$ ), the lower half space is given by symmetry. For TE polarization, we find directionality around  $\phi = 0$ , whereas in the TM case additional, smaller peaks occur. The ray in the left upper inset represents one typical trajectory emitting to  $\phi \approx 0$  (marked by arrows). The emitting bounce (marked 1, 1s is the symmetry-related counterpart), the three bounces before and the one after (marked 2) are shown. Whereas the trajectories are equal for both polarizations, their intensities are different:

As visible in the right inset, the rays escaping at 1 hit the line of the Brewster angle  $|\chi_B| = \arctan 1/n < \arcsin 1/n$ . In the TE case, transmission is nearly complete and no intensity can reach the next bounce 2. This causes the sharp decrease in the intensity that is more clearly visible in Fig. 2(b).

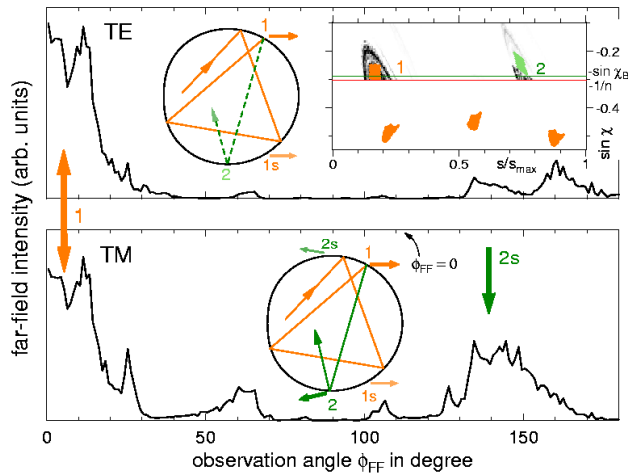


FIG. 3: (color online). Far-field emission pattern for TE (top) and TM polarization (bottom) calculated from an ensemble of rays on the unstable manifold in Fig. 2(b) and (c). Insets illustrate ray dynamics leading to directed emission. The dashed line has strongly reduced intensity due to reflection near the Brewster angle. Right inset: 250 rays were started in the rectangular region at 1 and followed forwards (region at 2) and backwards (the 3 regions below the critical line). 1s and 2s mark the symmetry-related bounces to 1 and 2.

The Fresnel law for TM polarization does not show the Brewster angle feature. Therefore, a significant percentage of the light is reflected towards bounce 2. Since bounce 2 emits into a different direction, an appreciable amount of intensity collects in a second far-field peak.

To summarize up to this point, we have seen that chaotic ray dynamics can lead to highly directional emission. However, the  $Q$ -factor is low since the light rays typically leave the cavity very quickly. Does this result of geometric optics carry over to the wave dynamics of the electromagnetic field?

It has been demonstrated that the FFP of optical modes can be strongly influenced by the unstable manifold of the underlying ray dynamics [28, 29, 31]. A consequence is that for fixed polarization and cavity parameters the FFP is independent on the internal mode structure [30]. This raises the hope that the high directionality observed in ray simulations of the limaçon cavity will survive in wave optics. To this end we solve Maxwell equations numerically using the boundary element method [34]. According to the discrete symmetry, even and odd modes are distinguished.

The top panel of Fig. 4 shows near- and far-field pattern of a high- $Q$  TE mode. The normalized frequency  $\Omega = \omega R/c = 26.0933$ ,  $c$  being the speed of light in vacuum, corresponds to, e.g., a free-space wavelength of about 900 nm for  $R = 3.75 \mu\text{m}$ . Indeed, as predicted by our ray dynamical analysis the mode exhibits directional light emission around  $\phi = 0$ . The angular divergence of  $24^\circ$  is significantly smaller than

the values reported for low- $Q$  disks [21, 22], and also less than in Ref. [24]. Moreover, for fixed polarization and cavity parameters, the FFPs of all high- $Q$  TE modes in this cavity have similar envelope even though the internal mode structure is in general different. This is exemplarily demonstrated in the upper panel of Fig. 4 for an odd-parity mode (dashed line) which is quasi-degenerate with the even-parity solution (solid line). Note that in other types of cavities the even- and the corresponding odd-parity solution have in general a different FFP [24]. For the high- $Q$  modes with TM polarization we also observe an FFP which is independent of the internal mode structure, but a slightly different one, see lower panel of Fig. 4.

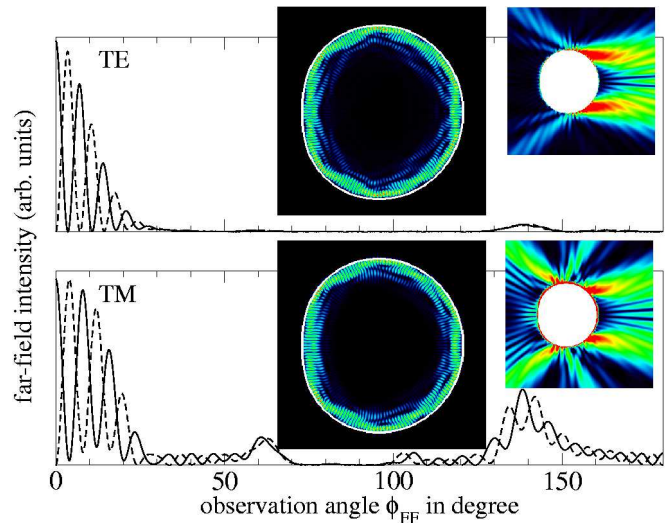


FIG. 4: (color online). Angular dependence of the far-field electric field intensity for a TE mode of even (top, solid line) and odd parity (top, dashed) with  $\Omega = 26.0933$ ,  $Q \approx 185\,000$ , and a TM mode of even (bottom, solid line) and odd parity (bottom, dashed) with  $\Omega = 25.8069$ ,  $Q \approx 10^7$ ; cf. Fig. 3. Insets contain the near-field pattern of even-parity modes (middle) and its external structure (right).

Whereas the ray and wave based FFPs in Figs. 3 and 4, respectively, agree remarkably well, other wave properties seem to contradict the ray simulations: (i) the mode does not look chaotic but spatially rather well confined. (ii) the cavity  $Q$ s are too large if compared to the escape rate from the chaotic repeller, in fact their values reach, or even exceed, the present limit achievable for microdisks with low residual absorption and surface roughness [9].

To further investigate the character of these optical modes we consider the Husimi projection [35], representing the wave analogue of the Poincaré SOS. From ray-wave correspondence one would expect that the Husimi projection is distributed uniformly over the unstable manifold. However, Fig. 5(a) demonstrates that the TE mode is localized around  $|\sin \chi| \approx 0.86$  and has only exponentially small intensity in the leaky region which explains the high  $Q$ -factor. A closer inspection [36] reveals that the mode intensity is enhanced around an unstable periodic ray trajectory (dots and inset in Fig. 5(a)) which is part of the chaotic repeller. This phenomenon is called scarring [27] and has been observed

in several kinds of physical systems including microcavities [37, 38, 39, 40]. Note that the other high- $Q$  modes found in this system also exhibit localization along – in general other – unstable periodic rays. The Husimi projection of the TM mode in Fig. 4 looks similar (not shown). The localization is even stronger, leading to a higher  $Q$ -factor.

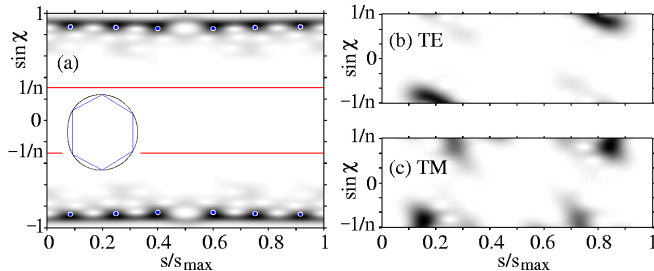


FIG. 5: (color online). (a) Husimi projection of TE mode in Fig. 4, cf. Poincaré SOS in Fig. 1(d) and unstable manifold in Fig. 2(a). The lines  $\sin \chi_c = \pm 1/n$  enclosing the leaky region are indicated. The dots mark the periodic ray trajectory illustrated in the inset. Magnified Husimi projection in the leaky region for the TE (b) and TM (c) mode; cf. Fig. 2(b) and (c) for the ray simulation results.

Even though the Husimi projection has an exponentially small contribution in the leaky region, it is precisely this outgoing light that determines the FFP. Figures 5(b) and (c) show the Husimi projection in the leaky region. The convincing agreement with the unstable manifold in Figs. 2(b) and (c) demonstrates its responsibility for the directional emission, whereas scarring guarantees the high  $Q$ -factor.

Note that, due to the observed agreement between ray and wave simulation, our results are also applicable to larger cavities. The particular deformation parameter  $\varepsilon = 0.43$  is the optimum value for the localization of the discussed FFPs with  $n = 3.3$  but highly localized FFP and high  $Q$ -factors can also be found for  $0.41 \lesssim \varepsilon \lesssim 0.49$  (not shown), i.e. fabrication tolerances are not crucial. Moreover, we tested that our results are robust against variations of the refractive index and remain valid for  $2.7 \lesssim n \lesssim 3.9$ .

In summary, we have proposed a deformed microdisk as a novel cavity design for robust directional light emission from high- $Q$  modes. No complicated adjustment of geometry parameters is necessary, and the emission directionality is largely independent from wavelength, cavity size, refractive index, and the details of the interior mode structure. The latter finding is especially relevant for multi-mode lasing devices. We trace our, at first sight, counterintuitive results back to (i) wave localization along unstable periodic ray trajectories ensuring high  $Q$ -factors and (ii) escape of rays along the unstable manifold of the chaotic repeller leading to directional emission. The simplicity of the cavity design allows for easy fabrication with a wide range of applications in photonics and optoelectronics. The discussed mechanisms are not restricted to disk-like geometries but can in principle also be exploited for other geometries such as deformed microspheres and microtori.

We thank E. Bogomolny, H. Kantz, T.-Y. Kwon, J. Nagler, and M. Robnik for discussions. Financial support by the Deutsche Forschungsgemeinschaft is acknowledged.

- 
- [1] K. J. Vahala, *Nature (London)* **424**, 839 (2003).
  - [2] H.-G. Park *et al.*, *Science* **305**, 1444 (2004).
  - [3] S. M. Ulrich *et al.*, *Phys. Rev. Lett.* **98**, 043906 (2007).
  - [4] P. Michler *et al.*, *Nature (London)* **406**, 968 (2000).
  - [5] J. Reithmaier *et al.*, *Nature (London)* **432**, 197 (2004).
  - [6] E. Peter *et al.*, *Phys. Rev. Lett.* **95**, 067401 (2005).
  - [7] M. Schwab *et al.*, *Phys. Rev. B* **74**, 045323 (2006).
  - [8] S. L. McCall *et al.*, *Appl. Phys. Lett.* **60**, 289 (1992).
  - [9] C. P. Michael *et al.*, *Appl. Phys. Lett.* **90**, 051108 (2007).
  - [10] L. Collot *et al.*, *Europhys. Lett.* **23**, 87 (1993).
  - [11] S. Götzinger *et al.*, *Nano Lett.* **6**, 1151 (2006).
  - [12] M. L. Gorodetsky, A. D. Pryamikov, and V. S. Ilchenko, *J. Opt. Soc. Am B* **17**, 1051 (2000).
  - [13] V. S. Ilchenko *et al.*, *Opt. Lett.* **26**, 256 (2001).
  - [14] A. A. Savchenkov, V. S. Ilchenko, A. B. Matsko, and L. Maleki, *Phys. Rev. A* **70**, 051804(R) (2004).
  - [15] A. C. Tamboli *et al.*, *Nature Photonics* **1**, 61 (2007).
  - [16] H. Lohmeyer *et al.*, *Eur. Phys. J B* **48**, 291 (2005).
  - [17] A. F. J. Levi *et al.*, *Appl. Phys. Lett.* **62**, 561 (1993).
  - [18] J. U. Nöckel and A. D. Stone, *Nature (London)* **385**, 45 (1997).
  - [19] C. Gmachl *et al.*, *Science* **280**, 1556 (1998).
  - [20] T. Tanaka, M. Hentschel, T. Fukushima, and T. Harayama, *Phys. Rev. Lett.* **98**, 033902 (2007).
  - [21] M. S. Kurdoglyan, S.-Y. Lee, S. Rim, and C.-M. Kim, *Opt. Lett.* **29**, 2758 (2004).
  - [22] M. Kneissl *et al.*, *Appl. Phys. Lett.* **84**, 2485 (2004).
  - [23] J. U. Nöckel, *Opt. Lett.* **19**, 1693 (1994).
  - [24] J. Wiersig and M. Hentschel, *Phys. Rev. A* **73**, 031802(R) (2006).
  - [25] H.-J. Stöckmann, *Quantum chaos* (Cambridge University Press, Cambridge, 2000).
  - [26] A. J. Lichtenberg and M. A. Leiberman, *Regular and Chaotic Dynamics* (Springer, Berlin, 1992).
  - [27] E. J. Heller, *Phys. Rev. Lett.* **53**, 1515 (1984).
  - [28] H. G. L. Schwefel *et al.*, *J. Opt. Soc. Am. B* **21**, 923 (2004).
  - [29] S.-Y. Lee, J.-W. Ryu, T.-Y. Kwon, S. Rim, and C.-M. Kim, *Phys. Rev. A* **72**, 061801(R) (2005).
  - [30] S.-B. Lee *et al.*, *Phys. Rev. A* **75**, 011802(R) (2007).
  - [31] S. Shinohara and T. Harayama, *Phys. Rev. E* **75**, 036216 (2007).
  - [32] M. Robnik, *J. Phys. A* **16**, 3971 (1983).
  - [33] H. Schomerus and M. Hentschel, *Phys. Rev. Lett.* **96**, 243903 (2006).
  - [34] J. Wiersig, *J. Opt. A: Pure Appl. Opt.* **5**, 53 (2003).
  - [35] M. Hentschel, H. Schomerus, and R. Schubert, *Europhys. Lett.* **62**, 636 (2003).
  - [36] R. Hegger, H. Kantz, and T. Schreiber, *Chaos* **9**, 413 (1999).
  - [37] S. B. Lee *et al.*, *Phys. Rev. Lett.* **88**, 033903 (2002).
  - [38] W. Fang, A. Yamilov, and H. Cao, *Phys. Rev. A* **72**, 023815 (2005).
  - [39] J. Wiersig, *Phys. Rev. Lett.* **97**, 253901 (2006).
  - [40] T. Fukushima, T. Harayama, and J. Wiersig, *Phys. Rev. A* **73**, 023816 (2006).